$$\varphi_3 = \mathrm{Tan}^{-1}\frac{\begin{pmatrix}\sin\varphi_1 \\ -S_2\cdot\sin\left(\sqrt{1-\varepsilon}\cdot\omega_1(T_R-2T_S)-\varphi_2\right)\\ \cdot e^{-\lambda_1(T_R-2T_S)}\end{pmatrix}}{\begin{pmatrix}\cos\varphi_1 \\ +S_2\cdot\cos\left(\sqrt{1-\varepsilon}\cdot\omega_1(T_R-2T_S)-\varphi_2\right)\\ \cdot e^{-\lambda_1(T_R-2T_S)}\end{pmatrix}}. \quad (39)$$

The solution (37) satisfies (36), and keeps the relation (29).

Solution in the period [4] ($t_T \leqq t$) :

In the period [4], $\dot{I}_0(t)$and $\ddot{I}_0(t)$ are

$$\dot{I}_0(t) = \ddot{I}_0(t) = 0\ . \quad (40)$$

The initial conditions in the period [4] is

$$\begin{cases} I_C(t_T) = I_C(t_T) \text{ in [3](37)} \\ \dot{I}_C(t_T) = \dot{I}_C(t_T) \text{ in [3](37)}\ . \end{cases} \quad (41)$$

From (40) and (41), $I_C(t)$ is solved as

$$I_C(t) = \frac{D_R}{\omega_1^2 T_S}\frac{S_4}{\sqrt{1-\varepsilon}}\cos\left(\sqrt{1-\varepsilon}\cdot\omega_1(t-t_T)-\varphi_4\right) \cdot e^{-\lambda_1(t-t_T)} \quad (42)$$

$$S_4 = \sqrt{1-2S_3\cos\left(\sqrt{1-\varepsilon}\cdot\omega_1 T_S+\varphi_1-\varphi_3\right)e^{-\lambda_1 T_S} + S_3^2\cdot e^{-2\lambda_1 T_S}} \quad (43)$$

$$\varphi_4 = \mathrm{Tan}^{-1}\frac{\sin\varphi_1 + S_3\sin\left(\sqrt{1-\varepsilon}\cdot\omega_1 T_S-\varphi_3\right)e^{-\lambda_1 T_S}}{\cos\varphi_1 - S_3\cos\left(\sqrt{1-\varepsilon}\cdot\omega_1 T_S-\varphi_3\right)e^{-\lambda_1 T_S}}. \quad (44)$$

The solution (42) satisfies (41), and keeps the relation (31).

COMPARISON TO THE SIMULATIONS

The first part of the solution $I_C(t)$ is plotted in Figure 7. The parabola smoothing time $T_S = 100$msec and the circuit parameters of (15) are assumed. In the lower two figures, the analytical solutions (black) and the LTSpice simulation results (red) are shown. They agree well, suggesting the validity of the analytical solutions.

As is shown in (16), the ripple $I_C(t)$ damps slowly. In the time range of Fig. 7, the amplitude is almost constant.

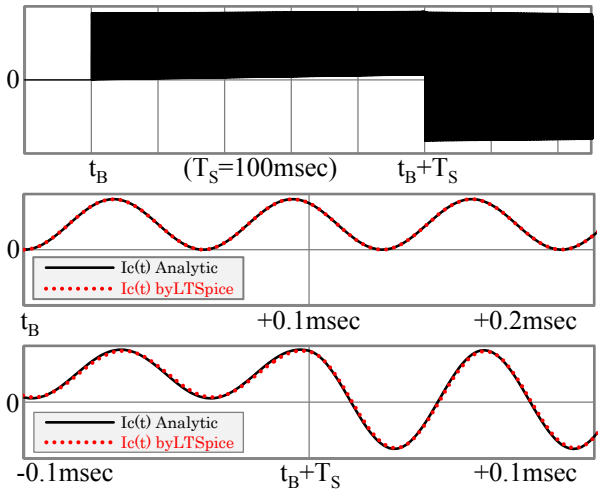

Figure 7: Top: The obtained ripple current $I_C(t)$ plotted for 150msec from the beginning of the current ramp t_B. Middle and bottom: The expanded plots for the 0.2msec period at t_B and $t_B + T_S$. The circuit parameters of (15) are assumed, where one cycle becomes 0.063msec.

DAMPED OSCILLATION AMPLITUDES

In the parabola periods [1] and [3], the solutions of $I_C(t)$ in (27) and (37) contain the constant term $(1-4\varepsilon)$ and the term proportional to the elapsed time. In the linear ramp period [2], the constant term $2\lambda_1 T_S$ is included in (32).

Apart from those terms, all the solutions from [1] to [4], marked in blue, contain the damped oscillation terms. If ε and φ_n (n: 1 to 4) are ignored due to their relatively small values, the damped oscillation term can be characterized by

$$S_n\cos\omega_1\Delta t\cdot e^{-\lambda_1\Delta t} \quad (45)$$

where S_n is the specific amplitude and Δt is the elapsed time of each period.

In the expressions of S_n, (33), (38), and (43), the cosine values are between -1 and 1. Hence the ranges of S_n become

$$\begin{aligned} 1-e^{-\lambda_1 T_S} &\leqq S_2 \leqq 1+e^{-\lambda_1 T_S} \\ |1-S_2 e^{-\lambda_1(T_R-2T_S)}| &\leqq S_3 \leqq 1+S_2 e^{-\lambda_1(T_R-2T_S)} \\ |1-S_3 e^{-\lambda_1 T_S}| &\leqq S_4 \leqq 1+S_3 e^{-\lambda_1 T_S} \end{aligned} \quad (46)$$

If, for example, $\lambda_1 = 0.5\mathrm{sec}^{-1}$ and $T_S = 0.1$sec, $e^{-\lambda_1 T_S}$ is close to unity because of the slow damping, and S_2 is

$$0.0488 \leqq S_2 \leqq 1.9512 \quad (47)$$

The value S_2 largely changes by a factor of up to 40 if the cosine value in (33), $\cos\left(\sqrt{1-\varepsilon}\cdot\omega_1 T_S\right)$, changes. The same property is applied to S_3, S_4, and to all the amplitudes in the following ramp cycles in Fig. 3.

In the J-PARC MR slow beam extractions, it is generally observed that the spill shapes, as is shown in Fig. 1, change every cycle to cycle of the MR acceleration. Sensitive fluctuations of S_n in connection to the cosine values will be the origin of this irreproducibility.

CIRCUIT PARAMETER DEPENDANCE

As are shown in the solutions (27), (32), (37), and (42), the ripple current $I_C(t)$ always has the form of

$$I_c(t) = \frac{D_R}{\omega_1^2 T_S}\{\ \cdots\ \} \quad (48)$$

where the terms inside the parentheses {} are the dimensionless numbers in the order of unity and define the dependence of ripple as a function of time.

Outside of the parentheses {} is the factor that signifies the magnitude of the ripple. Here this factor is defined as

$$I_{C0} \equiv \frac{D_R}{\omega_1^2 T_S} = L_1 C_1 \frac{D_R}{T_S}\ . \quad (49)$$

As is seen from (49), the ripple magnitude I_{C0} is proportional to the circuit inductance L_1, the capacitance C_1, the ramp rate D_R, and inverse of the parabola smoothing time T_S^{-1}.

In the originally designed requirements of MR, the expected current ripple is ~10^{-6} at the extraction [7]. The maximum designed bending magnet current is ~3000 A at 50 GeV. The corresponding ripple current is

$$3000\cdot 10^{-6} = 3\ \mathrm{mA} \quad (50)$$

Hence the ripple current I_{C0} should be in the order of mA.

Assuming simple numbers for example, from Table 1, as follows,

$$L_1 \sim 1000\ \mathrm{mH},\ C_1 \sim 1000\ \mathrm{nF},\ D_R \sim 1000\ \mathrm{A/sec},\ T_S = 0.1\mathrm{sec}, \quad (51)$$

then the ripple current I_{C0} becomes

$$I_{C0} = L_1 C_1 D_R / T_S \sim 10\ \mathrm{mA}\ . \quad (52)$$

The estimation of (52) shows that, although the expression of I_{C0} is based on the simplified circuit, Fig. 6, the derived LC oscillation current formula (49) properly represents the magnitude of the ripple current.

In the realistic MR case at present, however, the total capacitance of each magnet family is several times bigger than the sum of magnet capacitance. The cables used for the electrical connections of the magnets bring large capacitance into the circuit, as is shown in Table 1. The resulted ripple in (49) will be $I_{C0}\sim 30\text{mA}$ with $C_1\sim 3000\text{nF}$.

The beam ripple influence with the large capacitance is particularly severe in the injection periods when the beam size is large and the majority of the beam power loss is occurring. If the ramp down rate just before the injection period is assumed to be bigger than the ramp up rate as $D_R = 2000\ \text{A/sec}$, and $C_1\sim 3000\text{nF}$, then $I_c(t) \sim 60\ \text{mA}$. The bending magnet current at the injection period is ~200A, hence the ripple rate is $\sim 60\text{mA}/200\text{A} = 3\times 10^{-4}$. With an uncontrolled T_S, it may even reach 10^{-3}.

BUS BAR AND CABLE CAPACITANCE

Since the inductance is mainly defined by the machine dimensions such as magnet apertures or power line lengths, it's impossible to reduce L_1 in the I_{C0} .formula (49). The only possible way to lower the ripple is to reduce the capacitance of the entire circuit.

In order to fulfil this critical requirement, bus bar connections are commonly employed in the major proton synchrotrons, as are described in, for example, [3] and [6]. In bus bars, the capacitance per unit length is in general tens of times smaller than that of cables [8]. In fact, if the bus bar capacitance is estimated as co-axial conductors with an inner conductor radius r_i of 2cm and an outer conductor radius r_o of 0.5m, the capacitance per unit length C_0 becomes

$$C_0 \equiv 2\pi\varepsilon_0/\ln(r_0/r_i)\ \sim 17\ \text{nF/km}\ . \qquad (53)$$

The assumed outer radius r_o may differ from place to place in the synchrotron tunnel, but C_0 in (53) is generally insensitive to r_o when its size is assumed to be $\gtrsim 0.1\text{m}$.

In contrast to bus bars, high current cables have r_o only ~20% or so larger than r_i, resulting in a large factor of $1/\ln(r_0/r_i) > 5$. And there exists another factor multiplied, that is the relative permittivity of $\varepsilon'\sim 2.26$ for the crosslinked polyethylene insulation layer between the inner and outer conductors. As a result, the cable capacitance per unit length C_{Cable}, for example for the 500 mm^2 shielded cables [9] used for the MR bending and quadrupole magnets, becomes

$$C_{\text{Cable}} \equiv 2\pi\varepsilon'\varepsilon_0/\ln(r_0/r_i)\ \sim 740\text{nF/km}\ . \qquad (54)$$

The original design for the high current connection of the MR magnets is naturally by bus bars which have the same dimensions as the magnet's hollow conductors [8]. The design was kept for a while in the MR construction period [10] but later it was changed to the cables [11].

In the realistic case, the large cable capacitance is divided and scattered in the MR tunnel along with the magnets as in Figure 5, forming lots of minor current loops associated with the ripples of various LC oscillation frequencies. In the simplified treatment at present with a single load, the distributed feature of multiple loads is ignored. The expansion to the multiple element circuit is the next step subject and will be reported elsewhere.

RAMP PARAMETER DEPENDANCE

As is seen from (49), the ripple current $I_C(t)$ is related to the current ramp parameters as

$$I_C(t) \propto D_R/T_S\ . \qquad (55)$$

This factor appears in the right side of the circuit equation (8), $\ddot{I}_0 + 2\lambda_1\dot{I}_0$, as is seen in (22). This feature holds in the circuits with multiple loads, although its proof is skipped in this article. It is only pointed out here that the proportional expression (55) always holds in any circuit.

SUMMARY

The beam ripple generation mechanism in proton synchrotron magnet ramp currents is analytically investigated in a simplified circuit model.

It is revealed that the magnet current ripple is generated by the magnet current ramp itself, even if the ramp current as a function of time is mathematically ideal with no ripples. The magnitude of the resulting ripple current is proportional to the circuit capacitance and the ramp rate. The large capacitance and the faster ramp increase the ripples.

ACKNOWLEDGMENT

The author would like to thank Associate Professor M. Tomizawa, Dr. T. Kimura, and Dr. T. Shimogawa for the fruitful discussions and encouragements. The author also would like to thank all the people involved in the MR slow extraction beam development for their timeless efforts.

REFERENCES

[1] V. I. Veksler et al., "The 10 BeV proton synchrotron of the Academy of Science USSR," Atomic Energy, Vol. 1, Num. 4 (1956) 469; http://www.springerlink.com/content/r763155115r04167/

[2] M. Tomizawa et al., "PERFORMANCE OF RESONANT SLOW EXTRACTION FROM J-PARC MAIN RING," Proc. of IPAC'12, New Orleans, May 2012, to be published.

[3] S. Gilardoni et al., "Fifty years of the CERN PS Synchrotron Volume I," CERN-2011-004 (2011) 103; https://cdsweb.cern.ch/record/1359959

[4] L. Chapman et al., "OPERATION OF THE TEVATRON EXTRACTION SYSTEM," Proc. of PAC'85, Vancouver, May 1985, p. 3116; http://cdsweb.cern.ch/record/897635

[5] Datasheet of Toshiba TMEIC Corporation as of 2009 measurements.

[6] P. Zhang et al., "COMMON MODE NOISE ON THE MAIN TEVATRON BUS AND ASSOCIATED BEAM EMITTANCE GROWTH," Proc. of PAC'91, San Francisco, California, May 6-9, 1991, p. 93; http://accelconf.web.cern.ch/AccelConf/p91/PDF/PAC1991_0093.PDF

[7] M. Muto,"50 GeV Ring IGBT Power Supply and Ripples," Proc. of the Slow Extraction Meeting in Japan, Tanashi, Mar. 2000, KEK Proceedings 2002-15 (2003) p.131 (in Japanese).

[8] M. Muto, private communications.

[9] Hitachi Cable, Ltd. Cable Handbook: http://www.hitachi-cable.co.jp/ICSFiles/cable/ecocable/em_6000v_ce_f.pdf

[10] T. Oogoe, "J-PARC 50 GeV Proton Synchrotron Main Magnets Cablings," Proc. of the Meeting on the Technical Study at KEK, Tsukuba, Nov. 2006, KEK Proceedings2006-6 (2006) p.1 (in Japanese).

[11] T. Oogoe, "STATUS AND SCHEDULE OF J-PARC 50GEV SYNCHROTRON (3)," Proc. of the 4th Annual Meeting of Particle Accelerator Society of Japan, Wako, Japan, Aug. 2007, p.221 (in Japanese), http://www.pasj.jp/web_publish/pasj4_lam32/PASJ4-LAM32%20%28D%29/contents/PDF/WP/WP03.pdf